Quantum statistical mechanics via the recursive residue generation method[a]

Richard A. Friesner[b] and Robert E. Wyatt

Department of Chemistry and Institute for Theoretical Chemistry, The University of Texas, Austin, Texas 78712

Using the recursive residue generation method (RRGM), it is shown how Green's function matrix elements calculated in large basis sets ($N > 10^3$) can be utilized to obtain *controlled* approximations to average values, correlation functions, and power spectra in multimode anharmonic systems. Convergence of the method is demonstrated through studies on five and seven mode model systems with basis sets containing up to about 8×10^3 states.

I. INTRODUCTION

In recent years, there has been great interest in the calculation of quantum statistical properties of multidimensional systems. While a wide variety of methods exist (e.g., path integral techniques[1] and semiclassical approximations[2]), many important problems are still unresolved. This is particularly true for dynamical averages (e.g., time correlation functions and density matrix evolution), where reliable nonperturbative results have been obtained in general only for systems with a very small number of degrees of freedom, or where the Hamiltonian under consideration is extremely simple (e.g., harmonic).

We shall consider systems (molecules, molecular clusters) described by a parametrized effective Hamiltonian, typically with a small number of electronic levels coupled to a manifold of several vibrational degrees of freedom (and, perhaps, a perturbing probe like the radiation field). The most straightforward way to obtain a *controlled approximation* for quantum averages is direct diagonalization of the Hamiltonian expressed in a truncated basis set. Indeed, this is a standard way to verify results obtained from other approximation schemes. Unfortunately, the size of the matrix (N) grows rapidly with the number of degrees of freedom, and one soon runs out of memory in which to compute and store eigenvectors (which are required to compute statistical averages). The largest problems amenable to solution via direct diagonalization lead to Hamiltonian matrices with $N \leq 10^3$.

Recently, a new method (the recursive residue generation method, RRGM) of computing Green's function matrix elements which avoids any necessity for eigenvector calculation has been developed.[3-5] This permits the use of very large basis sets, and thus allows the direct approach to be extended to systems with an increased number of degrees of freedom. Numerical calculations show the method to be quite stable numerically even at very long time (hundreds of vibrational periods, for example). This

property is currently not shared by, e.g., time dependent path integral methods.[6]

We describe here implementation of the RRGM to calculation of quantum statistical averages. The general formalism is developed in Sec. II and a nontrivial numerical example (an anharmonic oscillator coupled to a multimode harmonic reservoir) is presented in Sec. III. We conclude by discussing anticipated further development of the approach.

The computational approach developed here does have limitations imposed by computer memory and time constraints. It can, however, serve a number of useful purposes: (1) Accurate quantum results can now be generated for sizable nontrivial systems, so as to test the results of less systematic approximations. (2) Direct application to experiments (where the observables usually are *averages*) is possible for small or medium-sized molecules. (3) The method can be combined with perturbation techniques to treat molecules embedded in condensed phases.[7] (4) Studies of fundamental questions like quantum chaos in multiphoton pumping[8] will be facilitated.

In related studies, Moro and Freed[9] have developed a recursive approach to the calculation of correlation functions and spectra in *classical* statistical systems. The Lanczos method was used to tridiagonalize complex-symmetric matrices for use in magnetic resonance line shape studies. They concluded that ". . . exceedingly difficult problems of large dimensions may be conveniently solved by using the Lanczos algorithm." In our quantum formulation, the Lanczos algorithm also plays a key role.

II. THEORY

A. General formalism

Consider a system described by a time-independent Hamiltonian H, a function of the various electronic and nuclear coordinates. The time autocorrelation function of an operator A (which yields spectra in the linear response limit) is given by

$$C(t) = \text{Tr}\{\rho(0)A(0)A(t)\}$$
$$= \text{Tr}\{\rho(0)A(0)e^{+iHt}A(0)e^{-iHt}\}, \tag{1}$$

where $A(0) \equiv A$ is the operator at time $t = 0$, and $\rho(0)$ is the initial density matrix. For the applications described here, we assume a canonical system, so that

$$\rho(0) = e^{-\beta H}/\mathrm{Tr}\{e^{-\beta h}\} = e^{-\beta H}/Q. \tag{2}$$

In addition, the nonequilibrium average of the operator is

$$\langle A(t) \rangle = \mathrm{Tr}\{\rho(t)A(0)\} = \mathrm{Tr}\{e^{+iHt}\rho(0)e^{-iHt}A(0)\}. \tag{3}$$

If we insert a complete set of states $\{|i\rangle\}$, $C(t)$ involves multiple summation [there is a similar expression for $\langle A(t) \rangle$]:

$$C(t) = \frac{1}{Q} \sum_i \sum_j \sum_k \sum_l \sum_m \langle i|e^{-\beta H}|j\rangle$$
$$\times \langle j|e^{+iHt}|k\rangle\langle k|A|l\rangle\langle l|e^{-iHt}|m\rangle\langle m|A|i\rangle. \tag{4}$$

Because of the invariance of the trace to the choice of representation, in all of these equations we are free to use any convenient basis set.

For most systems of interest, the sums in Eq. (4) can be truncated, for one or more of the following reasons: (a) thermal cutoff: $\langle i|\exp(-\beta H)|j\rangle \ll 1$; (b) time cutoff: $\langle i|\exp(\pm iHt|j\rangle \ll 1$; and (c) range cutoff: $\langle i|A|j\rangle \ll 1$. Thus, $C(t)$ can be computed from a *finite set* of matrix elements of the operators $e^{-\beta H}$, e^{iHt}, and A. The truncation limits can be increased systematically until a desired degree of convergence is achieved.

In the first stage of computation, the RRGM is used to compute accurate values of the thermal and time propagators, $\langle i|\exp(-\beta H)|j\rangle$ and $\langle i|\exp(-iHt)|j\rangle$. This is the most time consuming part of the calculation and is discussed in more detail in the next section. These elements are computed only once and are read into the high speed memory as they are needed. For a large class of relevant operators, including various products of coordinates (e.g., $q_i^r q_j^s$), the matrix elements of A are trivial. The final summations in Eq. (4) are then performed in such a way as to exploit any selection rules inherent in the operator A. Efficient indexing procedures ensure that only nonzero terms are evaluated. Storage requirements can also be minimized by efficient use of a state indexing algorithm.

B. Optimization of computation of Green function matrix elements

The RRGM is aimed at computing thermal or time Green functions $\langle i|\exp(\kappa H)|j\rangle$, where $\kappa = \beta(\equiv 1/kT)$ or $\kappa = \pm it$, in systems with very large bases ($N \geq 10^3$). In terms of the eigenvectors and eigenvalues of $H(H|a\rangle = E_a|a\rangle)$,

$$\langle i|\exp(\kappa H)|j\rangle = \sum_a \langle i|a\rangle\langle a|j\rangle\exp(\kappa E_a).$$

Instead of computing *all* eigenvalues and eigenvector coefficients ($\langle i|a\rangle$), the RRGM recursively generates the *largest* transition amplitudes $\langle i|a\rangle\langle a|f\rangle$ and their associated eigenvalues. The number of eigenvalues and transition amplitudes generated (N_{eval}) depends upon the number of steps taken in the recursion procedure, N_{rec}.

In general, $N_{eval} < N_{rec}$, since some "spurious" eigenvalues are generated, and then discarded.[3,10]

There are two important considerations in designing an RRGM code to calculate statistical averages. First, one would like to minimize the time spent in calculating each Green function, given that a specified level of accuracy in the final averages is desired. Secondly, the set of Green functions which must be computed should be restricted to be as small as possible. Each of these objectives presents substantial problems; the solutions adopted here are not necessarily optimal. In Sec. III B, this topic will be revisited in the context of a specific Hamiltonian.

The first decision is a choice of basis set. We adopt a direct product harmonic oscillator basis $|j\rangle = |a, \mathbf{n}\rangle$, where a labels the electronic state (if there is only one potential surface, this variable is unnecessary) and $\mathbf{n} = (n_1, \ldots, n_r)$, where $\{n_i\}$ are the usual phonon quantum numbers. The main advantage is that matrix elements of the potential energy are sparse and easily computed if $V(\mathbf{x})$ is a polynomial (it can be fit to one if a numerical representation is all that is available).

The most time consuming part of the RRGM is operating with the matrix H on the iterated state vector ($|u_n\rangle$ or $|v_n\rangle$, in the notation of Ref. 3). When H is a sparse matrix, orders of magnitude decreases in computer time can be attained. As long as $V(\mathbf{x})$ consists of products of functions of independent coordinates [e.g., $V(x_1, x_2) = f_1(x_1)f_2(x_2)$], the matrix elements $\langle n_i|f_1(x_1)|n_j\rangle$, $\langle n_i|f_2(x_2)|n_j\rangle$ can be stored in arrays and used to generate H internally. This avoids reading large numbers of matrix elements from secondary storage, typically an extremely slow process.

Once a basis set has been chosen, a portion of it, the *active space*, is selected to be used in computation of each matrix element G_{ij}. Because the active space can be easily shifted for each calculation, an optimized space can be constructed for each pair (i, j). This reduces the size of the basis used in each computation, and thus reduces time requirements considerably. Accuracy can be checked by systematic increase in the active space dimension, the requirements of which will be dependent upon the magnitude of the off-diagonal coupling elements and energy spacings of the basis functions. Minimization of off-diagonal coupling by a canonical transformation of the harmonic oscillator basis set (not attempted in the calculations reported here) is also possible, and should serve to decrease the active space size. The active space concept was not used in obtaining the results in Sec. III.

One great advantage of the RRGM is that computation time is virtually independent of the number of times or temperatures computed. [This is because most of the computation goes into the generation of a subset of amplitudes $\langle i|a\rangle\langle a|j\rangle$ and eigenvalues E_a in Eq. (4).] Hence, the technique is especially suitable for analysis of long-time behavior.

Selection of the Green function matrix elements to be calculated involves analysis of the specific Hamiltonian under study. Cutoffs in the total zero-order diagonal energy E_i^0 and in the quantal separation Δn_{ij} of two states are imposed, and then systematically increased until

convergence is achieved. The former is a relatively simple thermal criterion, while the latter depends on understanding the connections induced in the Hamiltonian by off-diagonal terms. An actual implementation of this procedure is described in Sec. III, where convergence of the desired average values is demonstrated.

III. APPLICATION TO A MODEL SYSTEM

A. Hamiltonian

In this section, numerical results will be presented for the following system: a field perturbed anharmonic oscillator is coupled to a multimode harmonic reservoir. In terms of raising and lowering operators for the anharmonic oscillator ($a^\dagger$, a) and the reservoir modes ($b_i^\dagger$, b_i) the Hamiltonian is

$$H = \hbar\omega_a[(a^\dagger a) - x(a^\dagger a)^2] + V_r[a^\dagger + a]$$

$$+ \sum_{i=1}^{n} \hbar\omega_i b_i^\dagger b_i + \sum_{i=1}^{n} V_i[a^\dagger b_i + ab_i^\dagger], \qquad (5)$$

where $\hbar\omega_a$ and $\hbar\omega_i$ are harmonic energy spacings in the anharmonic and the ith reservoir mode, x is the anharmonicity parameter, and V_r and V_i are parameters which control the strength of the field and intramolecular coupling. This Hamiltonian has been used previously in studies of laser molecule interaction,[3–5] chaos in multiphoton excitation,[8] and laser interaction with surface adsorbed species.[11] Numerical values for the parameters are listed in Table I. In contrast to earlier studies,[3–5] V_r has been assigned a large value, in order to create a highly perturbed energy level structure, the dynamics of which would be difficult to treat by conventional techniques.

The basis set chosen to represent the Hamiltonian contains products of harmonic oscillator functions for the $(n + 1)$ modes:

$$|i\rangle = |n_a\rangle|n_1\rangle \cdots |n_n\rangle,$$

where $n_j = 0, 1, \ldots$. Note that these states are eigenfunctions of the following part of the Hamiltonian in Eq. (5):

$$H^0 = \hbar\omega_a[(a^\dagger a) - x(a^\dagger a)^2] + \sum_{i=1}^{n} \hbar\omega_i b_i^\dagger b_i. \qquad (6)$$

If we allow a maximum of p states in each mode, then the total basis size is $N = p^{(n+1)}$. In most of the applications reported here, there are four reservoir modes ($n = 4$) and

TABLE I. Parameters in model Hamiltonian, Eq. (5).

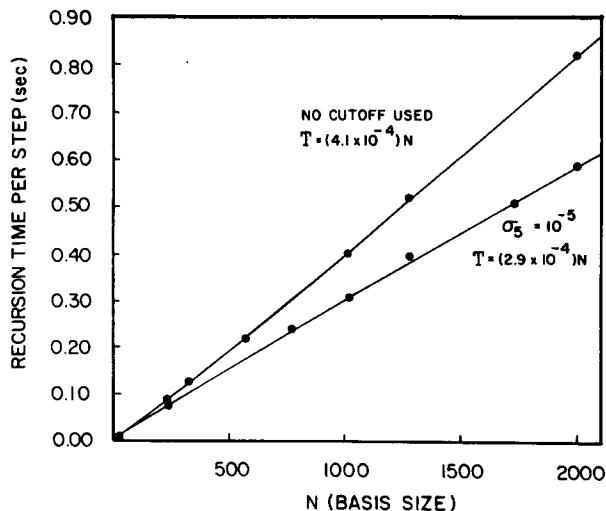| Seven mode system	
V_i ($i = 1, 6$)	100 cm^{-1}
Five mode system	
$\hbar\omega_a$	1000 cm^{-1}
$\hbar\omega_i$ ($i = 1, 4$)	1000 cm^{-1}
x	0.01
V_i ($i = 1, 4$)	30 cm^{-1}
V_r	300 cm^{-1}

FIG. 1. CPU time per Lanczos recursion step (on the CYBER 170/750) as a function of the basis size, with and without utilization of the cutoff parameter (σ_5).

$p = 3, 4, 5,$ or 6. This leads to bases with the dimension $N = 243, 1024, 3125,$ or 7776. However, some seven mode calculations, with $p = 3$ and $N = 2187$ are also reported.

B. Cutoff parameters

In order to achieve some degree of program optimization, variations in the following five parameters σ_1, $\ldots$, σ_5 were investigated. For a given basis (p, N are fixed), the first three parameters control the *number* of matrix elements, while the last two control the *accuracy* of each matrix element.

(1) Core cutoff. Let E_i^0 denote the (diagonal) energy for basis state i, $H^0|i\rangle = E_i^0|i\rangle$. Then if $E_i^0 > \sigma_1$, where σ_1 is a specified cutoff parameter, the matrix elements $G_{ij}(\beta)$ for "up transitions" $j \geq i$ are not computed. Of course, σ_1 must be allowed to increase as β decreases. The states $\{|i\rangle\}$ which satisfy this criterion define the set of *core states*.

(2) Membrane cutoff. If state i lies in the core, then in performing the trace operation in Eq. (4), a certain number of states [j, k, l, m in Eq. (4)] may have to be included, even though these states lie outside the core. However, if $E_j^0 > \sigma_2$ (where $\sigma_2 \geq \sigma_1$), we do not calculate $G_{ij}(\kappa)$. States excluded from the core, but satisfying the inequality $\sigma_1 < E_j^0 < \sigma_2$ lie in the *membrane*.

(3) Energy separation cutoff. Even if states i and j are such that $E_i^0 < \sigma_1$ and $E_j^0 < \sigma_2$, they may be too far apart—in energy separation—to produce large $G_{ij}(\kappa)$ values. So, if $|E_j^0 - E_i^0| > \sigma_3$, then the matrix elements are not computed. In systems with energy bands, this criterion is clearly designed to favor intraband transitions and transitions between neighboring bands.

(4) Shift vector cutoff. Let the quantum number vectors associated with states i and j be denoted $\mathbf{n}_i = (n_1, n_2, \ldots, n_r)$ and $\mathbf{n}_j = (n'_1, n'_2, \ldots, n'_r)$. Then the shift vector is $(\mathbf{n}_j - \mathbf{n}_i) = (\Delta n_1, \Delta n_2, \ldots, \Delta n_r)$, and the magnitude of the total shift is S_{ij},

TABLE II. Convergence of time correlation function.[a] (β = 0.002 cm^d; basis: p = 3, N = 243.)

N_{rec} Number recursion steps	σ_5 Cutoff parameter	$C (t = 1 \text{ ps})$[b]	Total CPU (s)[c]
30	10^{-4}	0.2031, −0.0368	368
40	10^{-4}	0.2382, −0.0362	523
50	10^{-4}	0.1523, −0.0152	682
30	10^{-5}	0.2518, −0.0243	379
40	10^{-5}	0.2448, −0.0405	536
50	10^{-5}	0.2374, −0.0385	694
50	10^{-8}	0.2332, −0.0354 ·	702
50	10^{-11}	0.2329, −0.0354	702
50	10^{-12}	0.2329, −0.0354	704
50	not used	0.2329, −0.0354	800
100	not used	0.2329, −0.0354	1611

[a] In *all* of the above cases: Q = 2.3007, $\langle x^2 \rangle$ = 0.68611, $C (t = 0)$ = 0.5866. For this set of parameters there are 282 diagonal and off-diagonal matrix elements, of which 151 are independent.
[b] Digits in error are underlined.
[c] Times for CYBER 170/750.
[d] Other parameter values: σ_1 = 2400 cm^{-1}, σ_2 = 2400 cm^{-1}, σ_3 = 1500 cm^{-1}, σ_4 = 2.0.

$$S_{ij} = \left| \sum_{k=1}^{r} \Delta n_k \right| .$$

If S_{ij} is too large, $G_{ij}(\kappa)$ tends to be small (due to bad Franck–Condon overlap), so G_{ij} is computed only when $S_{ij} < \sigma_4$.

(5) Recursion cutoff. A key step in the RRGM is used of Lanczos recursion[12] to generate a new basis, for each transition $i \rightarrow j$. The most time consuming step involves multiplication of an "old" recursion vector by nonzero elements of the Hamiltonian matrix H to obtain a new vector: $U_{new} = HU_{old}$. In order to speed up this multiplication, we skip the scalar multiplication step $(H)_{pq}(U_{old})_q$ if the qth element of U_{old} is sufficiently small; i.e., if $(U_{old})_q < \sigma_5$. Also, we want to keep the number of recursion steps (N_{rec}) as *small* as possible, and the value of σ_5 as *large* as possible, consistent with a given accuracy in the final averages. For a given value of σ_5, *too many* Lanczos recursion steps can lead to poor results, so preliminary comparisons need to be done to minimize the CPU time by decreasing N_{rec} and increasing σ_5. Numerical results illustrating this point will be presented in the next section.

C. Computation times and cutoff parameters

In this section, the use of σ_5 (which controls whether an element of H will be multiplied by an element of U_{old} in the Lanczos recursion method) to reduce computer time will be considered. First, when σ_5 is *not* used, the CPU time per recursion step is *linear* in N, as shown by the upper curve in Fig. 1. The total CPU time, for *one* Green function matrix element, is approximately

$$T = N_{rec}[AN + B], \tag{7}$$

where on the CYBER 170/750, $A \sim 4 \times 10^{-4}$ s and $B \sim 10 A$. The first term involving AN is the contribution (per recursion step) from the Lanczos method. The second term involving B arises from operations performed *after*

the Lanczos process is completed (this includes eigenvalue computation and sorting, and residue computation). It is noteworthy that the computation time per step, T/N_{rec}, is *linear* in the total basis size. For a fixed value of N, T is also linear in N_{rec}.

When σ_5 is introduced, the CPU time per recursion step decreases, because during the first few recursions there are many small values in the recursion vector U_{old}. An example is shown in Fig. 1, for σ_5 = 10^{-5}; the reduction in CPU time per step is about 25%. This value of σ_5 provides sufficient accuracy in the final averages.

Table II illustrates convergence of the time correlation function at t = 1 ps, $C(1)$, for one basis set (p = 3, N = 243). If σ_5 is "too large," σ_5 = 10^{-4}, the results are poor for all values of N_{rec}, but they become progressively worse as N_{rec} increases. However for N_{rec} = 50, cutoff parameters of 10^{-4}, 10^{-5}, 10^{-8}, 10^{-11}, 10^{-12}, and 0 (i.e., the cutoff option was bypassed) yield increasingly accurate values of $C(1)$. For the remaining calculations reported here, we chose N_{rec} = 50 and σ_5 = 10^{-5}, which provides a satisfactory compromise between high accuracy and low CPU time. With these choices, CPU times for calculations with three different bases are shown in Table III. The calculation of average values is segmented into

TABLE III. CPU times (s) on CYBER 170/750.

Basis		Parameters σ_1, σ_2 (cm^{-1})	Generate Green function files[a]	Compute average values
P	N			
3	243	2400	615	37
		3400	2 650	138
4	1024	2400	2 270	40
		3400	9 950	140
5	3125	2400	6 050	40
		3400	26 220	140
6	7776	2400	8 156	40

[a] Green functions were computed at 400 times and two temperatures.

TABLE IV. Dependence of average values, the time correlation function, and the spectral peak height upon basis size and parameter values.

Basis			β					
p	N	Parameters[a]	(cm)	Q	$\langle x^2 \rangle$	$Re[C(0)]$	C	I_{max}[b]
3	243	$\sigma_1 = \sigma_2 = 2400$ cm^{-1}	0.002	2.3007	0.6861	0.5640	0.159	1708.1
			0.004	1.5771	0.6075	0.5910	0.195	2868.5
3	243	$\sigma_1 = \sigma_2 = 3400$ cm^{-1}	0.002	2.4105	0.7125	0.6497	0.181	144.2
			0.004	1.5789	0.6085	0.5991	0.198	182.7
4	1024	$\sigma_1 = \sigma_2 = 2400$ cm^{-1}	0.002	2.3098	0.6929	0.5661	0.162	78.3
			0.004	1.5812	0.6105	0.5923	0.198	58.5
4	1024	$\sigma_1 = \sigma_2 = 3400$ cm^{-1}	0.002	2.4438	0.7302	0.6804	0.197	164.5
			0.004	1.5832	0.6128	0.6109	0.201	58.5
5	3125	$\sigma_1 = \sigma_2 = 2400$ cm^{-1}	0.002	2.3096	0.6928	0.5661	0.162	67.4
6	7776	$\sigma_1 = \sigma_2 = 2400$ cm^{-1}	0.002	2.3097	0.6927	0.5661	0.163	75.6
			0.004	1.5817	0.6107	0.5923	0.198	58.7

[a] Parameters not listed take the following values: $\sigma_3 = 1500$ cm^{-1}, $\sigma_4 = 2.0$, $\sigma_5 = 10^{-5}$, $N_{rec} = 50$.
[b] When $A = 1$ in Eq. (9), I_{max} is the maximum of $I(\omega)$ over the frequency range $[0, 250$ ps$^{-1}]$.

two major steps: production of a disk file of all Green function matrix elements, followed by assembly of these elements into average values.

D. Equilibrium averages

In this section, the dependence of Q, $\langle x^2 \rangle$, and $C(0)$ will be examined for different basis sets and for different choices of the parameters σ_i. The displacement coordinate in the anharmonic mode is x. In Table IV, these values are shown for two values of β (0.002 and 0.004 cm). First, for the lower temperature ($\beta = 0.004$ cm), with $\sigma_1 = \sigma_2 = 2400$ cm^{-1}, we observe convergence as p is increased from 3 to 6. However, the slight discrepancy between $\langle x^2 \rangle$ and $Re[C(0)]$ is due to incompleteness in the number of interacting states. When σ_1 and σ_2 are increased by 1000 cm^{-1} to expand the number of core states, the difference between $\langle x^2 \rangle$ and $Re[C(0)]$ decreases. Now, turning to the higher temperature ($\beta = 0.002$ cm), we note slightly larger differences between $\langle x^2 \rangle$ and $Re[C(0)]$; for example, $\{\langle x^2 \rangle - Re[C(0)]\}$ is 0.06 for $p = 3$, and 0.05 for $p = 4$ when $\sigma_1 = \sigma_2 = 3400$ cm^{-1}. However, these differences are smaller than for the restricted core ($\sigma_1 = \sigma_2 = 2400$ cm^{-1}).

The significant point about these results is that RRGM is a *controlled* route to converged statistical averages. As more states are allowed to interact, by expanding the basis (p) and/or the core and membrane (σ_1, σ_2) for each basis, we will converge to exact average values.

E. Correlation functions and power spectra

The time correlation function $C(t)$ for x was computed:

$$C(t) = (1/Q)\text{Tr}\{e^{-\beta H}xe^{+iHt}xe^{-iHt}\}. \qquad (8)$$

In addition, the power spectrum $I(\omega)$ was obtained from the Fourier transform of $C(t)$:

$$I(\omega) = A\left|\int_0^T e^{i\omega t}\Gamma(t)dt\right|^2,$$

$$\Gamma(t) = [C(t) - C]e^{-at^2}, \qquad (9)$$

where A is chosen to scale $I(\omega)$ (in practice, A is defined so that $I(\omega) = 1$ at its peak within the frequency range $[0, \omega_{max}]$). In Eq. (9), C is the long time average of the
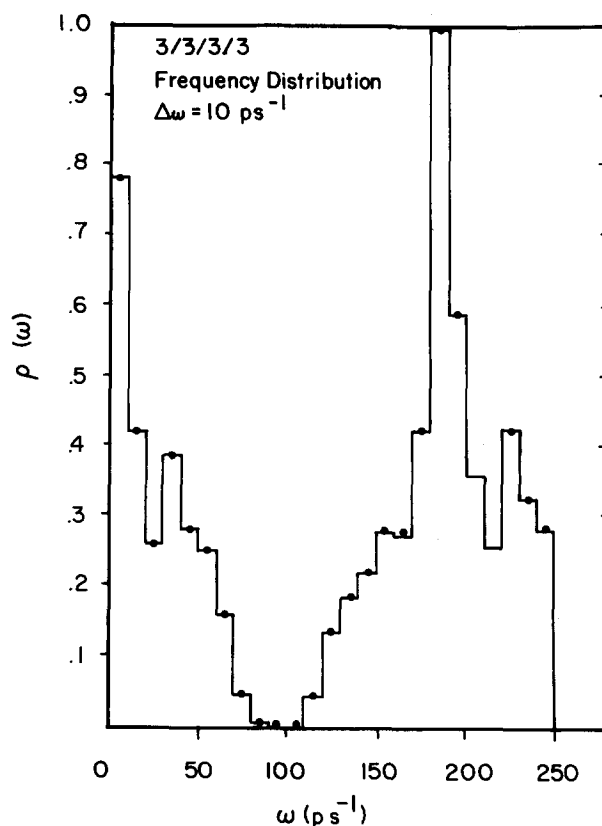

FIG. 2. Distribution of frequencies ($\omega = \Delta E/\hbar$) below 250 ps^{-1} for the Hamiltonian of Eq. (5) with the following basis: $p = 3$, $N = 243$. The maximum value has been scaled to unity. The values of ΔE were obtained by direct matrix diagonalization.

real part of $C(t)$; C represents a "DC shift" in the motion of the wave packet due to the anharmonicity in the Hamiltonian. The DC shift is subtracted from $C(t)$ so that very low frequency components will not dominate plots of the power spectrum. Our interest is in the dynamics relative to C, not the fact that the correlation function is shifted at long times. Finally, the Gaussian factor $\exp(-at^2)$ defines a "time window" which prevents relatively long times from entering into the calculation of $I(\omega)$. In practice, for the five mode systems, we chose a so that the correlation function was damped ($\sim$1% of the

$t = 0$ value) by $t = 1.5$ ps. (This condition requires that $a = 2$.) As expected, this damping factor introduces a slight broadening in each of the spectral lines. A range of different a values was investigated; however, the reported spectra are not highly sensitive to this value. In these calculations, $C(t)$ was computed at 400 time steps ($\Delta t = 0.004$ ps, and $I(\omega)$ was computed at 10^3 frequencies in the interval [0,250 ps^{-1}]. In addition, for the seven mode system, 800 time steps were used, and the effect upon $I(\omega)$ of different window cutoffs (varying a) was investigated.
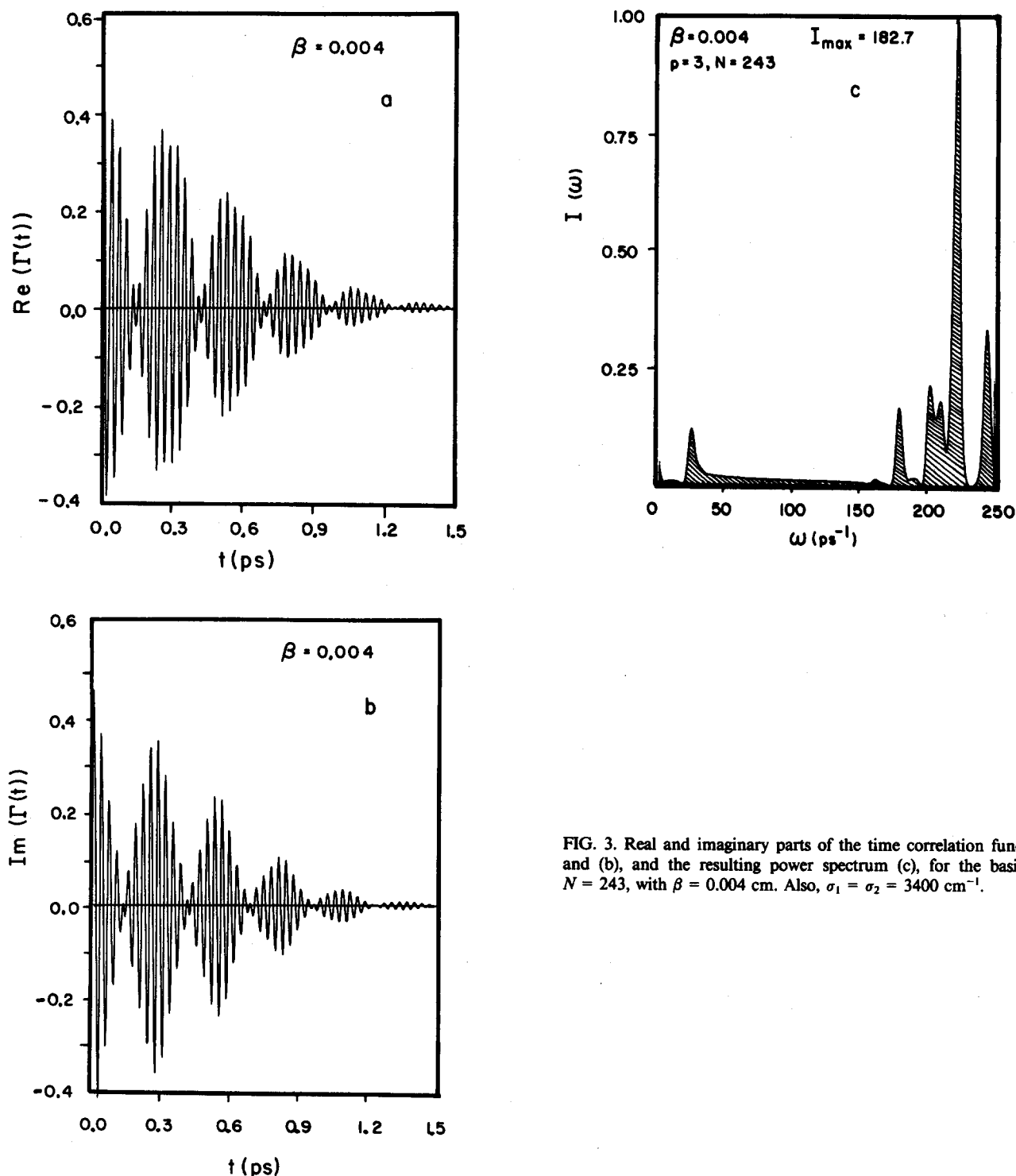

FIG. 3. Real and imaginary parts of the time correlation function, (a) and (b), and the resulting power spectrum (c), for the basis $p = 3$ $N = 243$, with $\beta = 0.004$ cm. Also, $\sigma_1 = \sigma_2 = 3400$ cm^{-1}.

For the parameters in this Hamiltonian, the states fall into bands separated by about 1000 cm^{-1}. Thus, in $I(\omega)$ there should be intense lines due to neighboring band transitions around $\omega = (1000\ \text{cm}^{-1})/(5.3\ \text{cm}^{-1}\ \text{ps}) = 200\ \text{ps}^{-1}$. In addition, intraband transitions contribute to lines at much lower frequencies. In order to obtain a more quantitative measure of the energy separations (frequencies) in systems of this type, we diagonalized H with $p = 3$ states in each mode, so that $N = 243$. The frequency distribution shown in Fig. 2 clearly shows peaks around 230, 190, and 40 ps^{-1}, in addition to the very low frequency peak from nearly degenerate states. However, since this "static" distribution does not reflect

the intensity of dynamical transitions, we now turn to $\Gamma(t)$ and $I(\omega)$.

Before considering results for this model Hamiltonian, we will examine some properties of $C(t)$ for a simple model which exhibits some features of the more complicated system. Consider a Hamiltonian with a nondegenerate ground state ($\epsilon_1 = 0$) and an excited level with two nearly degenerate states ($\epsilon_2 = \Delta$, $\epsilon_3 = \Delta + \delta$, $\delta \ll \Delta$). In the eigenvector representation,

$$C(t) = \frac{1}{Q} \sum_{j,k=1}^{3} e^{-\beta \epsilon_j} x_{jk}^2 e^{i(\epsilon_k - \epsilon_j)t}, \tag{10}$$
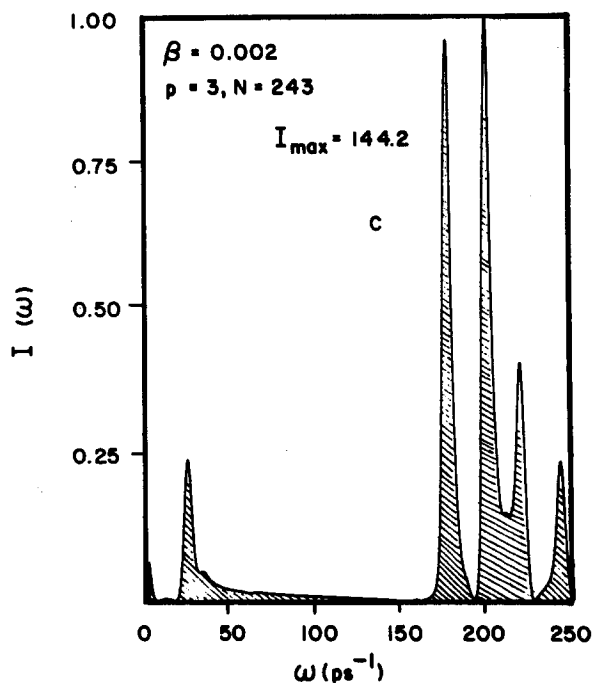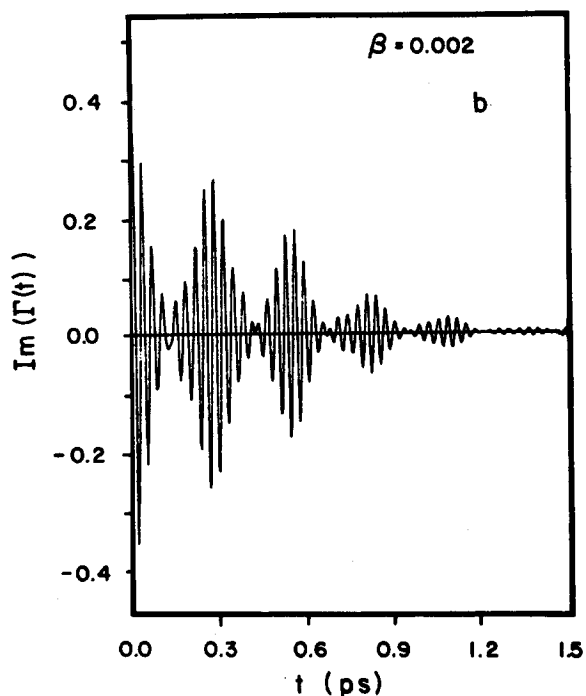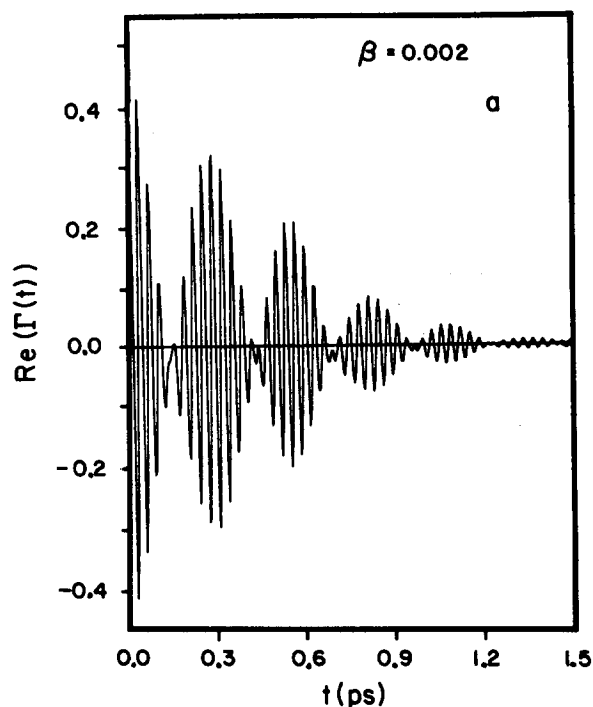
FIG. 4. See caption to Fig. 3; the only difference is that $\beta = 0.002$ cm.

where x_{jk} is a matrix element of the operator x. The real
and imaginary parts of $C(t)$ are

$$\mathrm{Re}(C) = (1/Q)\{x_{11}^2 + e^{-\beta\Delta}x_{22}^2 + e^{-\beta(\Delta+\delta)}x_{33}^2$$

$$+ x_{12}^2 F_\beta^+(\Delta)\cos(\Delta t) + x_{13}^2 F_\beta^+(\Delta + \delta)$$

$$\times \cos(\Delta + \delta)t + x_{23}^2 F_\beta^+(\delta)\cos(\delta t)\}$$

$$\mathrm{Im}(C) = (-1/Q)\{x_{12}^2 F_\beta^-(\Delta)\sin(\Delta t) + x_{13}^2 F_\beta^-(\Delta + \delta)$$

$$\times \sin(\Delta + \delta)t + x_{23}^2 F_\beta^-(\delta)\sin(\delta t)\}, \qquad (11)$$

where

$$F_\beta^\pm(\epsilon) = 1 \pm e^{-\beta\epsilon}.$$

Note the following characteristics of $C(t)$: (a) High inter-
band frequencies (Δ and $\Delta + \delta$) appear in $C(t)$ along with
the lower intraband frequency (δ). (b) At $t = 0$, $\mathrm{Re}(C)$
> 0, while $\mathrm{Im}(C) = 0$. (c) As t increases, $\mathrm{Re}(C)$ oscillates
about the positive value

$$C(\beta) = (1/Q)\{x_{11}^2 + e^{-\beta\Delta}x_{22}^2 + e^{-\beta(\Delta+\delta)}x_{33}^2\}.$$

In a harmonic system $C = 0$ because $x_{ii} = 0$, so C (the
DC shift) results from anharmonicity. (d) In the high T
limit ($\beta \rightarrow 0$), $F_0(\epsilon) = 0$, so that

$$\mathrm{Re}(C) = C(0) + \tfrac{2}{3}\{x_{12}^2 \cos(\Delta t)$$

$$+ x_{13}^2 \cos(\Delta + \delta)t + x_{23}^2 \cos(\delta t)\},$$

$$\mathrm{Im}(C) = 0.$$

These features (plus others) will be observed when we
examine correlation functions for the more complicated
Hamiltonian in Eq. (5).

We will now return to the model Hamiltonian in
Eq. (5). First, Fig. 3 shows $\mathrm{Re}[\Gamma(t)]$, $\mathrm{Im}[\Gamma(t)]$, and $I(\omega)$
for a relatively small basis ($p = 3$, $N = 243$), at a relatively
high value of β (0.004 cm), which corresponds to T
$= 362$ K. Some features of the three state model are
evident in these plots of $I(\omega)$, and in the power spectrum
shown in Fig. 3(c). The oscillation of $\mathrm{Im}[C(t)]$ about the
value zero, large values of $I(\omega)$ near $\omega = 200$ ps^{-1} due to
interband transitions, and less intense values for frequen-
cies below 50 ps^{-1} due to intraband transitions are clearly
evident. The high frequency oscillation in $C(t)$ has an
easily calculated period. Since $\Delta E^0 \sim 1000$ cm^{-1} for
these interband transitions, $\tau = 2\pi\hbar/\Delta E^0 \sim (30$ cm^{-1}
ps)/(1000 cm^{-1}) $= 0.03$ ps, a value close to what is
observed in Fig. 3(c). Continuing with results for the
same basis, Fig. 4 shows $\Gamma(t)$ and $I(\omega)$ for a lower value
of β (0.002 cm), which corresponds to $T = 725$ K.
Comparing the spectra in Figs. 3 and 4, we note that the
lines are more symmetric at the higher temperature.

Turning now to power spectra for a larger basis
($p = 4$, $N = 1024$), Fig. 5 shows $I(\omega)$ at the same two
temperatures. Although the values of Q and $\langle x^2 \rangle$ listed
in Table II are within a few percent for the two different
bases (e.g., $\langle x^2 \rangle = 0.7125$ for $p = 3$ and 0.7302 for p
$= 4$ when $\beta = 0.002$ cm), the power spectra are more
sensitive to changes in the basis set.

Finally, Fig. 6 shows both $\Gamma(t)$ and $I(\omega)$ when β
$= 0.004$ cm for the largest basis illustrated here: $p = 5$,
$N = 3125$. Except for slight differences in the frequency
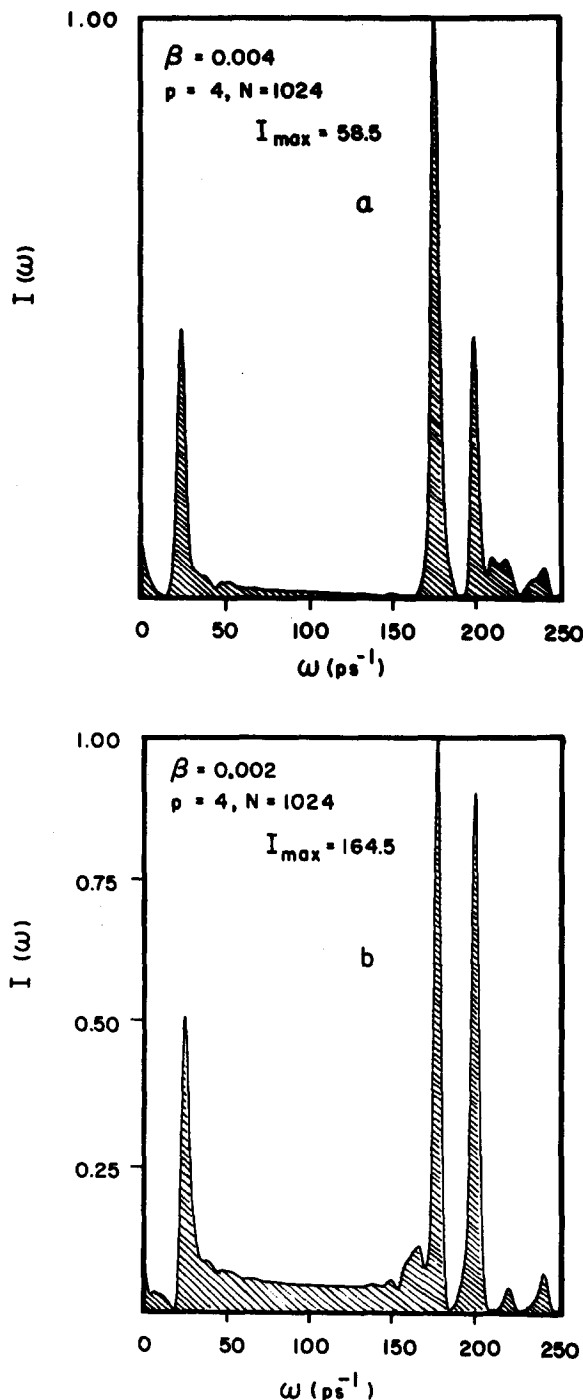range between 210 and 240 ps^{-1}, the power spectrum is

FIG. 5. Power spectra for the basis $p = 4$, $N = 1024$, at $\beta = 0.004$ cm
(a), and $\beta = 0.002$ cm (b). Also, $\sigma_1 = \sigma_2 = 3400$ cm^{-1}.

very similar to the low temperature result for $p = 4$, N
$= 1024$ in Fig. 5. This indicates that the power spectrum
in Fig. 5 is adequately converged for most interpretive
purposes. Other plots (not shown) for $N = 7776$ confirm
the convergence. It would be virtually impossible to study
the convergence of $I(\omega)$ for large basis sets ($N > 10^3$) with
any method but RRGM.

In order to investigate the influence of both the
number of bath modes and the Gaussian cutoff on the
power spectra, we studied a seven mode system with p
$= 3$ and $N = 2187$. Unlike the previous results, 800 time
steps were used to obtain the correlation functions and
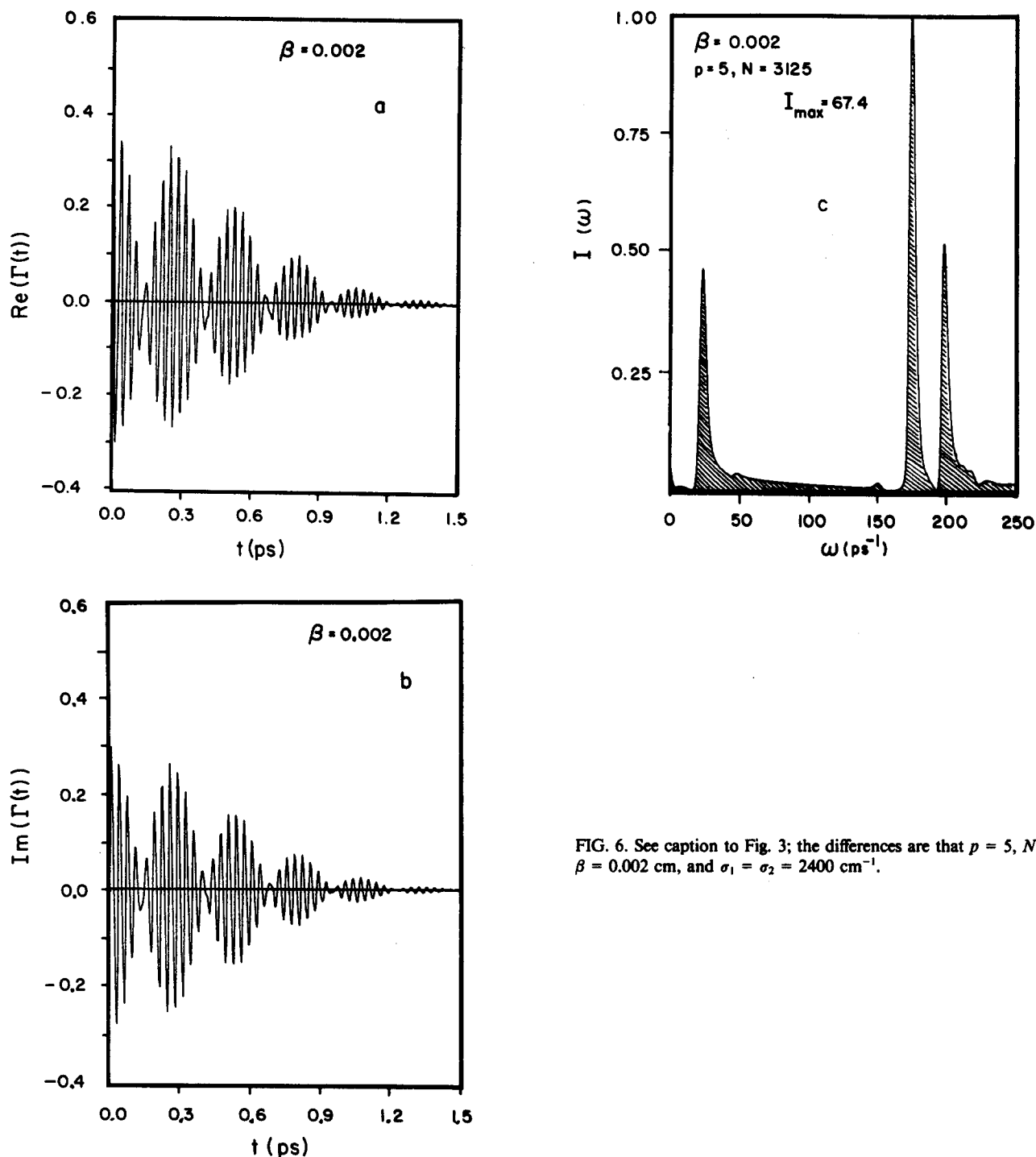power spectra. Figure 7 shows $I(\omega)$ for three values of the

FIG. 6. See caption to Fig. 3; the differences are that $p = 5$, $N = 3125$, $\beta = 0.002$ cm, and $\sigma_1 = \sigma_2 = 2400$ cm^{-1}.

cutoff parameter: $a = 0.5, 0.25$, and 0.0 (no cutoff). The absorption peaks are all of similar width, although the $a = 0$ spectrum [Fig. 7(c)] shows slightly sharper lines, with some "noise" between the peaks. (The noise is due to the correlation function not damping completely at the end of 800 time steps.) The main point is that use of a cutoff function did not lead to excessive broadening in the earlier plots for the five mode system.

One additional comment should be made concerning the power spectra shown in Figs. 3–6: The three peaks in each $I(\omega)$ plot arise from intraband transitions ($\omega \sim 30$ ps^{-1}) and nearest neighbor interband transitions ($\omega \sim 200$ ps^{-1}). Energies of the states in each band are split, so that transitions occur between upper (lower) states in

one band to lower (upper) states in the adjacent band. This leads to the two high frequency peaks ($\omega \sim 180$, 200 ps^{-1}) in each of these figures.

IV. CONCLUSION

In this study, we have demonstrated that direct computation of Green's function matrix elements in large basis sets ($N \gg 10^3$) can be utilized to obtain accurate results for quantum time correlation functions of a non-trivial multimode Hamiltonian.

The *controlled* nature of the approximations, permitting a systematic study of convergence, is evident and offers the possibility of producing definitive results for important model Hamiltonians of various types.
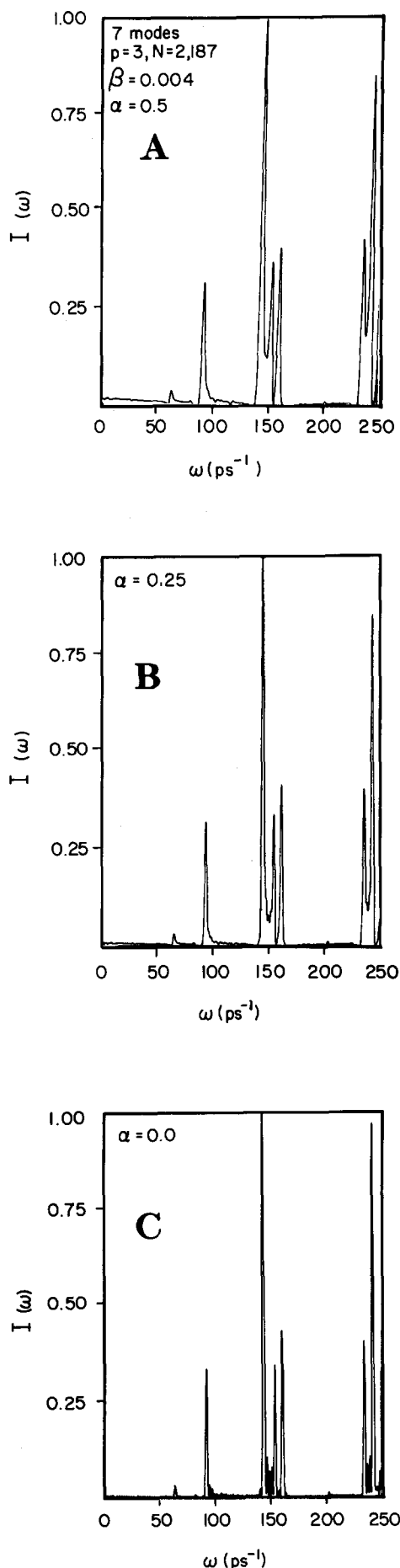
FIG. 7. Power spectra for a seven mode system with $p = 3$, $N = 2187$, for three values of the Gaussian cutoff parameter [see Eq. (9)].

A central issue that can be resolved by such a technique is the validity of applying various *uncontrolled* approximations to specific problems. For example, classical correlation functions are often assumed to accurately model the actual quantum correlation functions, under appropriate conditions. The questions are, what are the "appropriate conditions," and how good is the agreement?

For a one dimensional quartic oscillator, a recent calculation[13] indicates that even for relatively high temperatures ($\beta\hbar\omega \approx 2.0$), the classical time correlation function erroneously falls off much more rapidly than the exact (as determined by a converged basis set calculation) result. Using RRGM, this sort of comparison will now be possible for multidimensional potentials. A similar effort is aimed at studying the validity of path integral and semiclassical approximations.

It is currently feasible to apply the RRGM directly to experimental systems with a relatively small (1–10) number of relevant degrees of freedom and an accurately parametrized potential surface. Such work is currently in progress, e.g., for the CH_3F molecule.[14] Technical improvements in the computer code and implementation on a Class VI vector computer (e.g., CYBER 205 or CRAY 1) will exceed this capability, and is presently a high priority.

For very large molecules or condensed phase environments, the RRGM/SM approach must be combined with perturbative analytic methods. A straightforward way to do this is to select a set of *relevant* modes whose dynamics will be explicitly treated, and apply standard second-order time-dependent perturbative methods to the remaining degrees of freedom. This results in a set of Redfield-type equations[15] for the reduced density matrix. The advantage over conventional treatments of this type is that the system Hamiltonian contains many more states, and, hence, most of the dynamical recurrences of interest; the memory kernel of the bath is then correctly treated by a Markoff approximation. Solution of these equations via the RRGM will appear in subsequent publications.[7]

[1] P. Wolynes and D. Chandler, J. Chem. Phys. **74**, 4078 (1981); K. S. Schweitzer, R. M. Stratt, D. Chandler, and P. Wolynes, J. Chem. Phys. **75**, 1347 (1981); D. Thirumulai and B. J. Berne, J. Chem. Phys. **79**, 5029 (1983); R. Kuharski and P. J. Rossky, Chem. Phys. Lett. **103**, 357 (1983).

[2] D. W. Noid, M. L. Koszykowski, and R. A. Marcus, Annu. Rev. Phys. Chem. **32**, 267 (1981); I. Percival, Adv. Chem. Phys. **36**, 1 (1977); E. J. Heller, Acc. Chem. Res. **1410**, 368 (1981).

[3] A. Nauts and R. E. Wyatt, Phys. Rev. Lett. **51**, 2238 (1983).

[4] A. Nauts and R. E. Wyatt, Phys. Rev. A **30**, 872 (1984).

[5] J. Castillo and R. E. Wyatt (to be published).

[6] E. C. Dehrman, G. A. Jongward, and P. G. Wolynes, J. Chem. Phys. **79**, 6277 (1983).

[7] S. Hill, R. F. Friesner, and R. E. Wyatt (to be published).

[8] J. R. Ackerhalt, H. W. Galbraith, and P. W. Milonni, Phys. Rev. Lett. **51**, 1259 (1983).

[9] G. Moro and J. H. Freed, J. Phys. Chem. **84**, 2837 (1980); J. Chem. Phys. **74**, 3757 (1981); **75**, 3157 (1981).

[10] J. Cullum and R. A. Willoughby, J. Comput. Phys. **44**, 329 (1981).

[11] M. S. Slutsky and T. G. George, Chem. Phys. Lett. **57**, 474 (1978).

[12] C. Lanczos, J. Res. Natl. Bur. Stand. **45**, 255 (1950); R. Haydock, Solid State Phys. **35**, 215 (1980).

[13] R. Friesner (unpublished results).

[14] L. Campbell, J. Chang, and R. E. Wyatt (to be published).

[15] A. G. Redfield, Adv. Magn. Reson. **1**, 1 (1965).